Proceedings of the ASME 2020
Internal Combustion Engine Division Fall Technical Conference
ICEF2020
November 1-4, 2020, Denver, CO, USA

SAND2020-4832C

ICEF2020-3034

ASSESSMENT OF SPARK, CORONA, AND PLASMA IGNITION SYSTEMS FOR GASOLINE COMBUSTION

Sayan Biswas, Isaac Ekoto[1]
Sandia National Laboratories
Livermore, CA

Dan Singleton
Transient Plasma Systems, Inc.
Torrance, CA

Kristapher Mixell
Tenneco, Inc.
Plymouth, MI

Patrick Ford
Ford Motor Company
Dearborn, MI

ABSTRACT

In the present study, the performance and emissions characteristics of three low-temperature plasma (LTP) ignition systems were compared to a more conventional strategy that utilized a high-energy coil (93 mJ) inductive spark igniter. All experiments were performed in a single-cylinder, optically accessible, research engine. In total, three different ignition systems were evaluated: (1) an Advanced Corona Ignition System (ACIS) that used radiofrequency (RF) discharges (0.5 – 2.0 ms) to create corona streamer emission into the bulk gas via four-prong electrodes, (2) a Barrier Discharge Igniter (BDI) that used the same RF discharge waveform to produce surface LTP along an electrode encapsulated completely by the insulator, and (3) a Nanosecond Repetitive Pulse Discharge (NRPD) ignition system that used a non-resistor spark plug and positive DC pulses (~10 nanoseconds width) for a fixed frequency of 100 kHz, with the operating voltage-controlled to avoid LTP transition to breakdown. For the LTP ignition systems, pulse energy and duration (or number) were varied to optimize efficiency. A single 1300 revolutions per minute (rpm), 3.5 bar indicated mean effective pressure (IMEP) homogeneous operating point was evaluated. Equivalence ratio (ϕ) sweeps were performed that started at stoichiometric conditions and progressed toward the lean limit.

Both the ACIS and NRPD ignition systems extended the lean limit (where the variation of IMEP < 3%) limit ($\phi = 0.65$) compared to the inductive spark ($\phi = 0.73$). The improvement was attributed to two related factors. For the ACIS, less spark retard was required spark as compared to spark ignition due to larger initial kernel volumes produced by four distinct plasma streamers that emanate into the bulk gas. For the NRPD ignition system, additional pulses were thought to add expansion energy to the initial kernel. As a result, initial flame propagation was accelerated, which accordingly shortens early burn rates.

Keywords: Corona ignition, plasma ignition, nano-second repetitive pulsed ignition, spark ignition, advanced ignition system.

NOMENCLATURE

ϕ	Equivalence ratio
ϕ'	Charge mass equivalence ratio
ACI	Advanced compression ignition
aTDC	After top dead center
B	Bore diameter [m]
CA	Crank angle referenced to main TDC [°]
CA50	50% cumulative burn angle
CO	Carbon monoxide
CO_2	Carbon dioxide
COV	Coefficient of variation
DI	Direct injection
EGR	Exhaust gas recirculation
EVC/EVO	Exhaust valve close/open

[1] Contact author: iekoto@sandia.gov

DI	Direct injection
HC	Hydrocarbon
HRR	Heat release rate [J/°CA]
H/C	Hydrogen-to-carbon ratio
IMEP	Indicated mean effective pressure
ITE	Indicated thermal efficiency
IVC/IVO	Intake valve close/open
LHV	Lower heating value [kJ/g]
$\boldsymbol{m}$	Mass [kg]
$\mathbf{N_2}$	Nitrogen
NO	Nitric oxide
NOx	Nitrogen oxide
NVO	Negative valve overlap
$\mathbf{O_2}$	Molecular oxygen
PID	Proportional, Integral, Derivative
PM	Particulate matter
PVO	Positive valve overlap
RGF	Residual gas fraction
RON	Research octane number
rpm	Revolutions per minute
SACI	Spark assisted compression
SI	Spark ignition
SOI	Start of fuel injection
ST	Spark timing
$\boldsymbol{T}$	Temperature [K]
T10/T50/T90	10%, 50%, and 90% boiling points
TDC	Top dead center
Subscripts	
$\boldsymbol{air}$	Air
$\boldsymbol{f}$	Fuel
$\boldsymbol{int}$	Intake
$\boldsymbol{main}$	Main intake charge
$\boldsymbol{stoich}$	Stoichiometric condition

1. INTRODUCTION

Future engine automotive efficiency gains will require the transition of spark-ignited (SI) gasoline engine combustion towards more challenging dilute regimes [1]. Lean-burn SI can improve part-load efficiency due to a reduction in throttling from increased charge mass and reduced wall heat transfer losses from lower combustion temperatures [2-4]. Lower combustion temperatures likewise reduce the production of nitrogen oxide (NOx) pollutant emissions. Cycle thermodynamic efficiency is also increased by higher charge specific heat ratios that result from increased air dilution. Finally, fuel-lean operation is very amenable to the use of various advanced compression ignition (ACI) strategies where some amount of the charge mixture is consumed by auto-ignition rather than a flame [5]. As a result, shorter burn durations lead to more effective work extraction. To maintain stable, knock-free combustion across the entire load-speed map, mixed-mode operation can be employed where ACI is utilized for part-load and boosted SI for high power-density conditions [6-8]. An ACI variant – spark assisted compression ignition (SACI) strategy is beneficial here at low-to-moderate loads, where some amount end-gas auto-ignition is induced by compressive heating by a combination of the compression stroke and pressure-rise from the spark deflagration.

Regardless of the lean-burn strategy employed, some amount of mixture inhomogeneity is generally required for stable combustion. Specifically, fuel-rich regions created by late-cycle direct injections are needed in the vicinity of the igniter in order to produce strong and repeatable deflagration events. However, these fuel-rich regions also lead to an associated increase in engine-out NOx and particulate matter (PM) emissions. Moreover, three-way catalysts commonly used to control NOx emissions are ineffective for even small amounts of excess oxygen in the exhaust stream. Accordingly, the challenge for lean-burn combustion systems is to limit the required amount of fuel stratification.

Fuel stratification can be significantly reduced or even eliminated through the use of various advanced low-temperature plasma (LTP) ignition devices. Conventional point-source thermal ignition systems (i.e., inductive spark ignition) fail to achieve repeatable ignition in lean mixtures due to slow and highly stochastic early burn rates [9-12]. Advanced LTP ignition systems, however, increase the lean ignition limit through some combination of increased initial ignition volume and early kernel energy from successive discharge events [13-16]. A key requirement for these LTP systems is to avoid inter-electrode breakdown to other engine surfaces as elevated temperatures (10,000 K+) can lead to severe electrode erosion.

Two electrical pulse generation strategies are commonly employed to create the LTP responsible for ignition. The first is radiofrequency (RF), where alternating current (AC) waveforms with frequencies on the order of 1 MHz and voltage amplitudes of 15 kV+ are applied for up to 2 milliseconds. Strong reduced electric fields (E/N) lead to extensive fast-gas heating, ionization, and dissociation [17]. The RF pulse generation strategy is most suitable for bulk-gas corona streamer formation or surface streamer formation along dielectric surfaces. The second is nanosecond repetitively pulsed discharges (NRPD), where positive direct current (DC) discharges with pulse-widths of 10s of nanoseconds are pulsed at frequencies up to 100 kHz. In addition to the corona and surface streamer discharges described above, NRPD enables the use of opposed anode and cathode configurations that result in electric field enhancement in the vicinity of both electrodes, but without the transition to breakdown due to the short pulse duration. As a result, more ionization and fast gas heating are possible, which is favorable for radical generations [18, 19].

Depending on the electrode configuration, both RF and NRPD igniters can produce multiple ignition sites responsible for a faster and more complete burn than conventional spark ignition [16, 20, 21]. Moreover, these igniters have been used to extend dilution tolerance limits through the formation of active radicals that shorten ignition delays [12] and rapid volumetric heating via electron energy transfer processes [22-24]. However, few studies have directly compared the performance of these systems for a common engine platform and operating point.

In the present study, performance and emissions characteristics of three different ignition systems that generate LTP via either RF or NRPD discharge strategies were compared to inductive spark in a single-cylinder, optically accessible, research engine. Two RF ignition systems were evaluated: 1) Advanced Corona Ignition System (ACIS) and 2) Barrier Discharge Ignition (BDI) system. The third ignition system utilized NRPD with a conventional non-resistor spark plug. Experiments were performed in a 0.55-liter single-cylinder research engine at a 3.5 bar indicated mean effective pressure (IMEP) operating condition, with the engine speed fixed at 1300 revolutions per minute (rpm). Lean stability limits were experimentally determined for all igniters along with the associated improvement in indicated thermal efficiency (ITE).

2. EXPERIMENTAL SETUP

All experiments were performed in a 4-valve, single-cylinder, research engine. Engine specifications were described in detail in previous studies [25, 26]; hence, only a brief description is presented here. The engine head features central injection and spark, with a spray-guided piston bowl. A centrally located Bosch injector (HDEV 1.2) with 8 uniformly spaced nozzles with a diameter of 125 µm forming a 60° spray angle was used to deliver fuel. A single early fuel injection at 330 crank angles (CA) before top dead center (TDC) was used to create a homogenous fuel/air mixture in the cylinder. The geometric compression ratio was set to 13:1.

Intake and exhaust cam timings were set to produce a positive valve overlap (PVO) of 34 CA centered at TDC of the exhaust stroke. The PVO generated moderate residual gas fractions of between 17.5 and 22.3%., which led to mild charge heating. Engine speed was fixed at 1300 rpm through the use of a motoring dyno, with an optical encoder (0.1 CA resolution) used to measure crank location. Intake ports were designed to minimize swirl and tumble flows, and hence reduce turbulence driven heat transfer losses. A water-based Aquatherm heat exchanger was used to keep the cylinder wall and engine head to 90°C. Table 1 summarizes major engine specifications, including geometry, valve, injection and spark timing (ST), and other relevant operating characteristics.

A Kistler 6135A piezo-electric pressure sensor was used to measure the cylinder pressure data that was used to obtain the heat release rate and IMEP. A two-zone model was employed for heat release analysis based on the measured cylinder pressure. The two-zone model divided the combustion chamber into two separate regimes – burned and unburned, assuming complete combustion in the burned regime. The modified Woschni correlation optimized for lean gasoline compression combustion [27] was used to estimate heat loss from the combustion chamber since end gas auto-ignition was evident for all test conditions.

TABLE 1. Engine specifications and operating conditions.

Displaced volume [cm^3]	551
Bore/Stroke/Connecting Rod [mm]	86/95.1/ 166.7
Geometric Compression Ratio	13:1
Intake Valve Open/Close [CA]†	343 / -145
Exhaust Valve Open/Close [CA]†	160 / -343
Valve Lift [mm]	9.7
Fuel Pressure [bar]	100
Injector Hole Number	8
Injector Cone Angle [°]	60
Injector Orifice Diameter [µm]	125
Intake Pressure [kPa]	53 – 78
Exhaust Pressure [kPa]	105
Intake Temperature [°C]	42
Engine Speed [rpm]	1300
Cycle fueling rates [mg/cycle]	13.8 – 15.4
Equivalence ratio	0.59 – 1
Charge mass equivalence ratio	0.49 – 0.75
Residual gas fraction [%]	17.5 – 22.3
Spark Timing	-52 – -15
Main SOI [CA]†	-330

†0 CA corresponds to TDC of the compression stroke

Research-grade RD587 gasoline fuel with a research octane number (RON) of 92.1 and an octane sensitivity (OS) of 7.3 was utilized in the present study. Key physical and thermodynamic properties are summarized in Table 2.

TABLE 2. Properties of research-grade RD587 gasoline.

Liquid Density @15 °C [g/L]	748
LHV [MJ/kg]	41.9
H/C ratio	1.972
O/C ratio	0.033
Research Octane Number	92.1
Octane Sensitivity	7.3
T10 / T50 / T90 [°C]	57 / 98 / 156

A Tescom ER5000 PID (Proportional, Integral, Derivative) pneumatic flow controller was used to precisely regulates the intake air supply. Intake and exhaust runners were heated using resistive heaters and insulated using fiberglass insulation pads. A Chromalox circulation heater located between the intake runner and air supply stream was employed to hear the intake charge up to 42°C. Intake pressure was varied between 53 – 78 kPa to achieve target lean fuel/air conditions. First, the initial

pressure was set to achieve stoichiometry and decreased in gradual, steady steps to reach the lean-limit. The lean-limit was marked by the onset of unstable combustion, where the coefficient of variation (COV) of IMEP was greater than 3%. Exhaust pressure was fixed at 1.05 bar.

Emission measurements were carried out by sampling gases from the exhaust plenum and feeding them to emission analyzers via a heated tube. CAI 600 NDIR/Oxygen Multi-Component analyzer was used for carbon monoxide (CO), carbon dioxide (CO_2), and O_2 measurements. Unburned hydrocarbon (HC) was measured using a CAI 600 HFID analyzer. Combustion efficiency was estimated, combining the CO and HC emission measurements with injected fuel per cycle and airflow rates. A CAI 600 HCLD NO/NOx chemiluminescence analyzer was used to measure NOx emissions; however, NOx emission was not reported since the authors suspect the values were erroneous due to a discovered blockage in the emissions sampling line; CO, CO_2, and O_2 measurements are believed to be unaffected. These measurements will be repeated at a later date. A schematic of the engine setup and emission measurement system is shown in Figure 1.

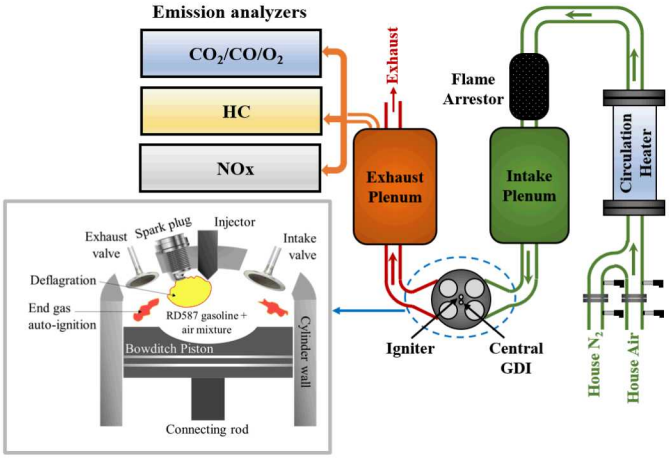

FIGURE 1. Schematic of the engine, emission analyzers, and combustion processes.

In the present study, three different advanced ignition systems were evaluated: 1) radio frequency (RF) advanced corona ignition system (ACIS), 2) RF barrier discharge ignition (BDI) system, and 3) nanosecond repetitive pulse discharge (NRPD) system. For ACIS and BDI systems, the pulse energy (voltage) and pulse duration were varied to optimize the combustion process. For the NRPD transient plasma ignition system, pulse number and energy were varied to optimize engine performance. The spark ignition system utilized a high-energy inductor coil that supplied a single pulse with a fixed energy of 93 mJ. Figure 2 illustrates the three different advanced igniters, and a brief description of each ignition system is presented below.

1) **Advanced Corona Ignition System (ACIS):** The Tenneco corona ignition employed high-frequency AC RF in the order of 1 MHz and voltages in the order of 20 kV or more. The ACIS igniter features a 4-prong electrode that generates four high-energy, long, and very repeatable corona streamers that emanate into the combustion chamber. The streamer strength depends on the applied voltage and pulse duration. The primary voltage ranged between 20 – 35 V with a pulse duration between 500 – 2000 µs.
2) **Barrier Discharge Ignition (BDI) system:** BDI system utilized the same Tenneco hardware that was used to produced ACIS. The BDI electrode has a hemispherical shaped tip where the anode was covered by high-dielectric strength aluminum oxide. The electrode configuration resulted in the formation of surface discharge streamers that completely surrounded the insulator during discharge. Previous studies have shown [28, 29] that radical formation results from these surface discharges, which can lead to larger and faster ignition kernels. For the BDI system, the primary voltage range was much higher than the ACIS system (50 – 75 V) with a shorter pulse duration (500 – 1000 µs).
3) **Nanosecond Repetitive Pulse Discharge (NRPD) system:** A Transient Plasma Systems Inc. SSPG-101-HF high-voltage pulse generator was used to create positive DC pulses with a peak voltage of 17 kV and pulse duration of full-width at half max (FWHM) of around 10 nanoseconds at a fixed 100 kHz frequency. The operating voltage was controlled to avoid breakdown. A Brisk long reach J-hook type non-resistor spark plug was connected to the pulse generator system via a high-voltage feedthrough connector (Caton LGG 31-HD receptacle).

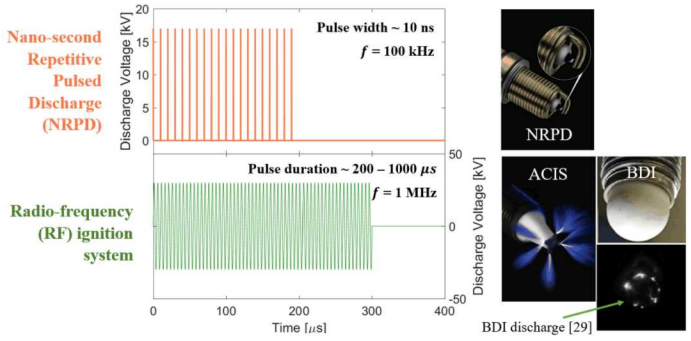

FIGURE 2. Example voltage waveforms for the NRPD and RF (ACIS, BDI) ignition systems.

For each experiment, the engine was motored for around 30 seconds, followed by 120 seconds of firing with the desired fueling schedule, ST, and ignition system settings (pulse voltage and duration/number) to allow engine combustion chamber

surfaces to warm up and emissions measurements to stabilize. Ignition system settings and ST were adjusted iteratively until the target IMEP of 3.5 bar was achieved with the lowest fueling rate possible while also maintaining the ringing intensity (RI) below 1 MW/m^2 and NOx emissions below 5 g/kg-fuel. If necessary, ignition system settings were also adjusted to avoid breakdown transition that can lead to electrode erosion or insulator puncturing. Once control variables were optimized, 100 cycles worth of data were collected. The engine was then motored, with the entire process repeated for the next operating condition.

3. RESULTS AND DISCUSSION

The results and discussion section is divided into four parts. The first part discusses the performance parameters and characteristics of the different ignition systems. The effect of pulse voltage (primary for the RF pulse generator and secondary for the NRPD pulse generator) and pulse duration (or the number of pulses for the NRPD pulse generator) on combustion performance was evaluated in the second part. The third part compares the emissions performance with the use of the different ignition systems. Finally, combustion behavior with optimized igniter settings and timings were compared for a common lean combustion condition.

Profiles of cylinder pressure and heat release rate (HRR) produced by combustion initiated by each of the ignition systems are plotted in Figure 3 for common equivalence ratios. The figures on the top are for a baseline stoichiometric (i.e., $\phi = 1.0$) condition, while profiles on the bottom are for conditions at the lean stability limit for the spark ignition system (i.e., $\phi = 0.73$). For the stoichiometric condition, ITE and COV for the NRPD and BDI systems are comparable to that of the spark igniter, with HRR profiles that are fairly similar. Note that combustion with all igniters evaluated featured a moderate amount of end-gas auto-ignition, as evidenced by the sharp second HRR peak that follows the initial deflagration period. We attribute this in part to the retained residuals and heat from the modest PVO. The ACIS, on the other hand, produced a modest increase in ITE (30.1% for spark and 31.2% for ACIS), which from the HRR profile can be attributed to shorter burn durations with combustion phasing centered closer to TDC.

For the $\phi = 0.73$ condition, ITE increased by roughly 2 points with all ignition systems. Once again, the BDI produced similar ITE as did the spark igniter, while NRPD and ACIS produced a 0.6- and 0.8-point increase respectively. Despite similar combustion phasing produced by each ignition system, the NRPD and ACIS had significant spark retard of 7 and 10 CA, respectively, relative to the spark igniter. Finally, it is notable that while end-gas evidence of end-gas auto-ignition is clearly apparent in all 4 HRR profiles, the end-gas auto-ignition peak is most prominent for the HRR profiles that resulted from ACIS ignition. Evidence of end-gas auto-ignition is less prominent, but still evident for the condition with NRPD ignition. But for the HRR produced by both spark and BDI ignition, the deflagration and auto-ignition contributions were less distinct, which is likely because the averaged HRR profiles were much more variable.

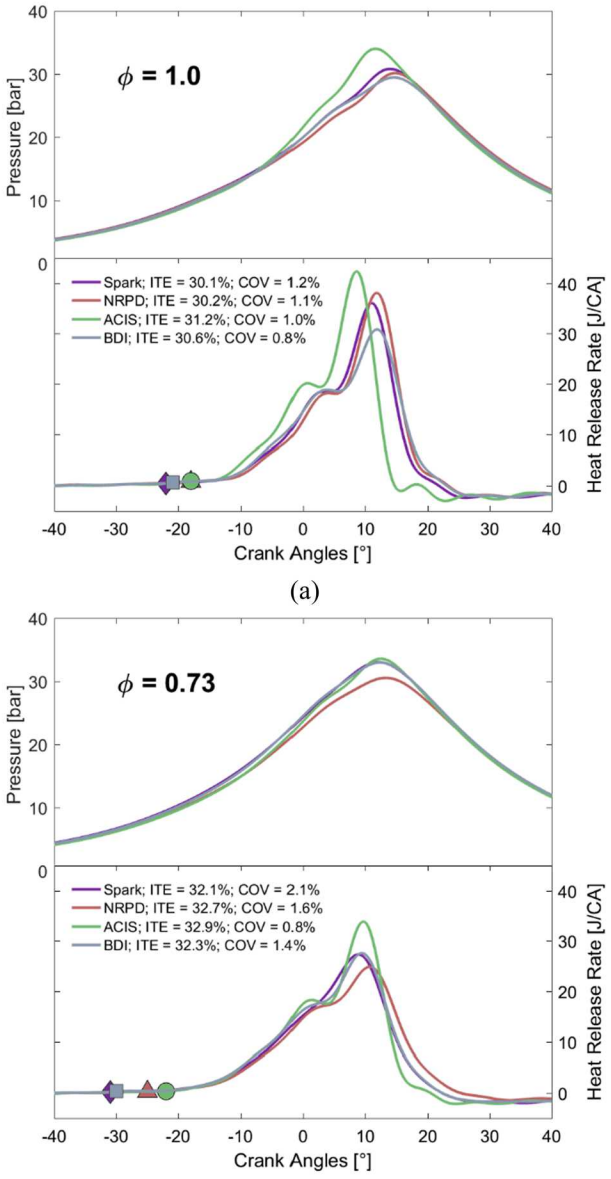

FIGURE 3. Cylinder pressure and heat release rate profiles of (a) $\phi = 1.0$, (b) $\phi = 0.73$ for 1300 rpm, 3.5 bar IMEP condition. The markers indicate the spark timing.

The influence of pulse number for NRPD and pulse duration for ACIS on HRR behavior is illustrated in Figure 4 for a fixed lean operating condition ($\phi = 0.65$). In Figure 4 (a) it is evident from the HRR profiles that increased NRPD pulse number (i.e., from 10 to 30 pulses) led to shorter combustion durations with more prominent and repeatable end-gas auto-ignition. As a result, COV was reduced from 10% with 10 pulses to only 1.7% with 30 pulses, a value comparable to COV at the stoichiometric condition in Figure 3 (a). Similarly, HRR profiles produced from

the use of the ACIS in Figure 4 (b) illustrate that longer pulse durations likewise led to shorter combustion durations and improved COV. However, the relative improvement was less than what was observed for increased pulse number with NRPD. The reason is that undesirable breakdown event was detected with the longer durations. Accordingly, longer durations required lower primary voltages to avoid breakdown, which as a consequence, meant there was less energy available for ignition.

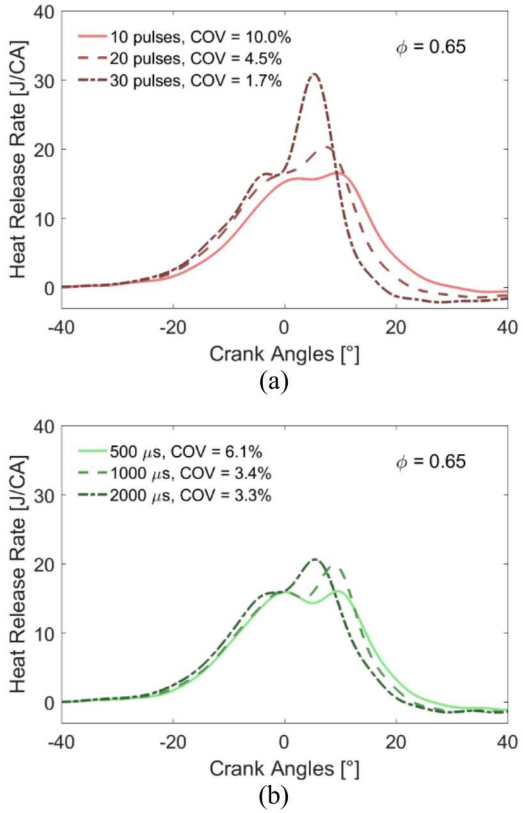

FIGURE 4. The effect of (a) number of pulses for NRPD ignition, (b) pulse duration for ACIS.

To better understand why increased pulse duration with ACIS was less effective than increased pulse number with NRPD at reducing combustion variability, in-cylinder density has been plotted in Figure 5 (a) for 3 different ϕ (i.e., $\phi = 0.98, \phi = 0.80, \phi = 0.65$) as a function of crank angle for the time period between 70 and 10 CA before TDC. Also on the plot is a yellow star that denotes the optimal ST for each ϕ; the profile $\phi = 0.65$ condition features ST for both the moderate and long pulse durations (i.e., 1000 and 2000 µs). As can be observed in the plot, the in-cylinder density at a given CA is higher for lower ϕ due to the higher amount of retained charge mass with increased dilution, and is partially balanced by the required ST advance needed to for leaner mixtures. As ϕ lowers from 0.98 to 0.80, the cylinder density and the time of discharge is nearly the same. However, when ϕ is further lowered to 0.65, the ST advance required more than offsets the higher initial charge mass, which accordingly limits the duration. If longer durations are desired, the pulse voltage must accordingly be lowered to avoid breakdown due to the lower charge density (and hence lower E/N), which leads to a weaker initial kernel, which requires additional ST advance to avoid breakdown, and so on. As a result, the impact of increased duration is essentially offset by lower discharge voltage.

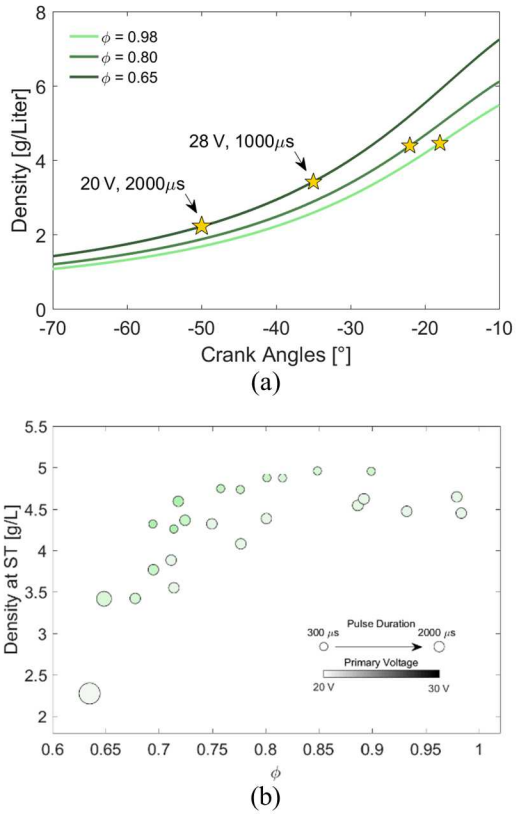

FIGURE 5. The effect of cylinder density on (a) ST, (b) ignition parameters (pulse energy and pulse duration) setting.

Plots of the density at ST as a function of ϕ are plotted in Figure 5 (b) for all conditions from the ϕ sweep for the ACIS system. The shade of the marker is proportional to the primary voltage, while the size of the marker is proportional to the pulse duration. From these plots, it is evident that in-cylinder density is at ST is relatively invariant until $\phi = 0.72$. Beyond that point, the prevalence of arcing to the adjacent injector results in required compromise in pulse duration, and voltage is expected to lead to deleterious combustion performance, as will discussed shortly.

Measured ITE, COV, and combustion efficiency are plotted for the ϕ-sweep in Figure 6 for all LTP igniters and are directly compared to the spark ignition results. The same plot framework used in Figure 5 (b) is adopted here. For clarity, ACIS and BDI results are plotted separately from the NRPD results. Note that for the plots of COV with the LTP igniters, a solid line is used to represent the impact on stability for a baseline pulse duration of 500 µs for BDI and ACIS, and a baseline pulse number of 10 for

the NRPD. The dashed line denotes what happens if the pulse duration or number of pulses are optimized.

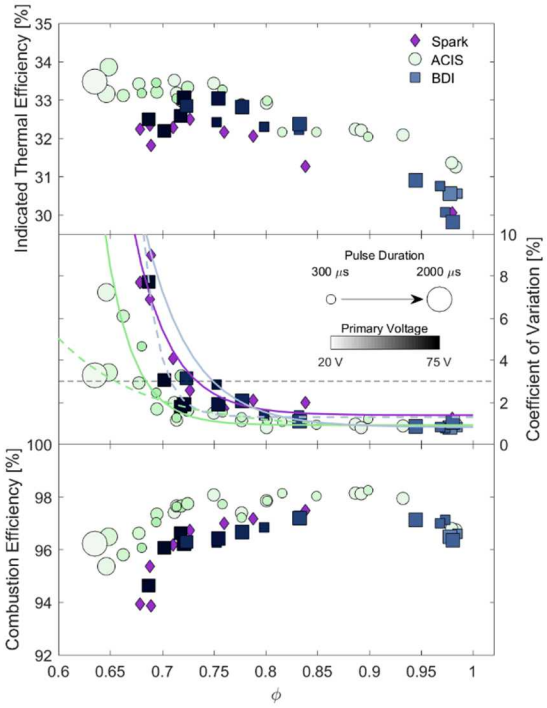

(a)

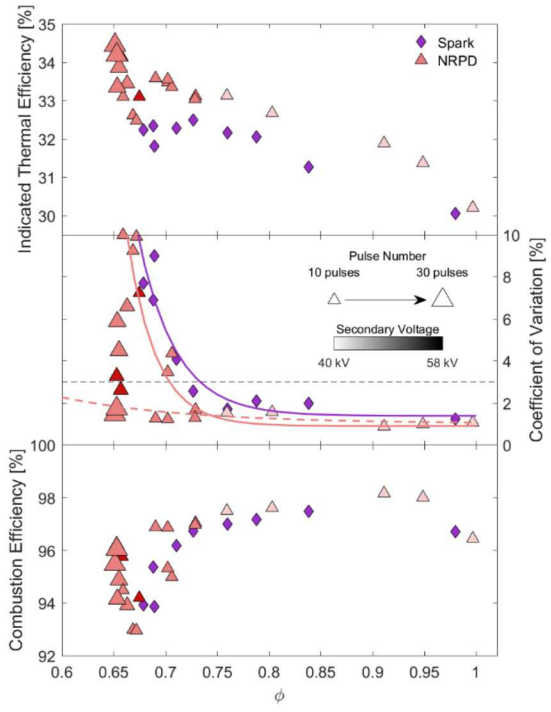

(b)

FIGURE 6: Comparison of (a) (ACIS, BDI) and (b) NRPD ignition system relative to inductive spark in terms of ITE, COV, and combustion efficiency as a function of equivalence ratio for 3.5 bar IMEP with fixed 1300 rpm engine speed.

It is immediately evident in Figure 6 (a) that there was virtually no difference in stability limits or cycle efficiency for the BDI relative to the spark ignition system. However, it should be cautioned that other researchers have observed that pre-strike events – where early discharges are performed in the intake stroke – can extend stability limits through favorable radical generation (likely ozone) [28].

Conversely, in the same figure, it is evident that ACIS extended the lean stability limit from $\phi = 0.73$ to $\phi = 0.68$ as compared to the inductive spark. The result was an increase in peak ITE from 32.5% to 33.8%, with a decrease in NOx by 30% (not shown here). There was a modest extension with pulse voltage and duration optimization, but the results were modest for the reasons described above. Finally, the 0.5 to 1.0 ITE point increase with ACIS relative to the inductive spark for a fixed ϕ noted in Figure 3 was consistently observed for all ϕ, which was in part due to slightly improved combustion efficiency, as can be observed in the bottom plot.

Finally, NRPD produced the largest extension of stable ignition limits with a lean stability limit of $\phi = 0.65$, as can be observed in Figure 6 (b). In fact, the lean-stability limit was never reached during the limited test window, as stability could continuously be improved by increased pulse number as described previously. Peak ITE for the NRPD was accordingly highest at 34.5%.

For each ignition system, Figures 7 plots a comparison of optimized ST, initial burn duration (CA10 – ST), and 50% burn angle (CA50) used as a proxy for combustion phasing. As shown in Figure 3, the optimized ST at the stoichiometric condition was nearly identical for all ignition systems evaluated, with similar initial burn duration and combustion phasing. The exception was the ACIS system, which produced notably shorter early burn durations and earlier combustion phasing. For leaner mixtures, combustion phasing steadily advanced, and CA50 values for a given ϕ remained tightly clustered for all ignition systems. Relative to the inductive spark igniter, significant spark retard of between 5 and 20 CA achieved with ACIS due to a comparable reduction in early burn duration. Moreover, the amount of achievable spark retard increased with leaner mixtures until the arc limit described previously was reached. The NRPD enabled a more modest amount of spark retard (3 to 10 CA) with more retard for leaner mixtures, while there was virtually no difference in ST or early burn duration for the BDI.

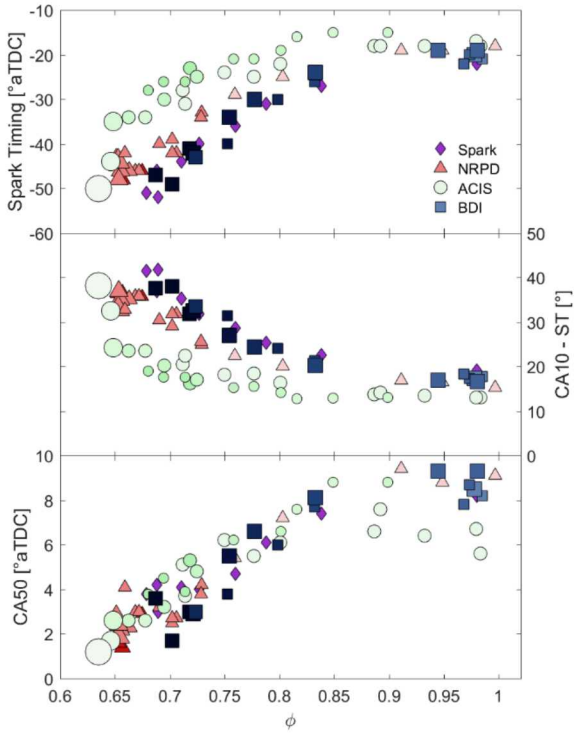

FIGURE 7. Comparison of optimized ST, CA10 – ST, and CA50 for the NRPD, ACIS, and BDI, along with benchmark data from the inductive spark ignition.

Figure 8 plots CO and HC emissions for ignition produced from the use of each ignition system across the ϕ-sweep along with a comparison of combustion efficiency. As expected, HC emission increased with decreasing ϕ for all ignition systems due to slower reaction rates. Conversely, CO emissions were highest near stoichiometry. It is believed to be due to modest charge inhomogeneity that resulted from incomplete vaporization of the impinged fuel spray during injection that led to locally rich regions where complete CO conversion to CO_2 was not possible. For leaner mixtures, CO emissions decreased drastically as these regions had sufficient O_2 for more complete CO-to-CO_2 oxidation. Finally, there was little variation in CO and HC emissions for the ignition systems, with the exception of the ACIS. The faster early burn rates resulted in more complete fuel-energy conversion across the ϕ-sweep, as can be observed in the plots of combustion efficiency.

Finally, HRR profiles for combustion from ignition by NRPD and ACIS, as well as the reference inductive spark are provided in Figure 9 at a fixed lean equivalence ratio ($\phi = 0.69$). Optimized ST is also denoted by a symbol for each igniter. Note that for the spark data, the condition was considered unstable with an extremely high COV of 9%. From the inset close-up HRR plot include, it is evident that despite the substantial ST retard with the use of ACIS and NRPD igniters relative to the spark, heat release rates were roughly equivalent by around 10 CA before TDC. For the ACIS, the behavior is attributed to larger initial ignition kernel volumes produced by 4 ignition sites at each prong. Conversely, NRPD was thought to have a comparable initial kernel volume to the spark as the gap sizes are equivalent. However, authors speculate that additional pulses after ignition deposited energy into the burned gas, which resulted in additional kernel expansion.

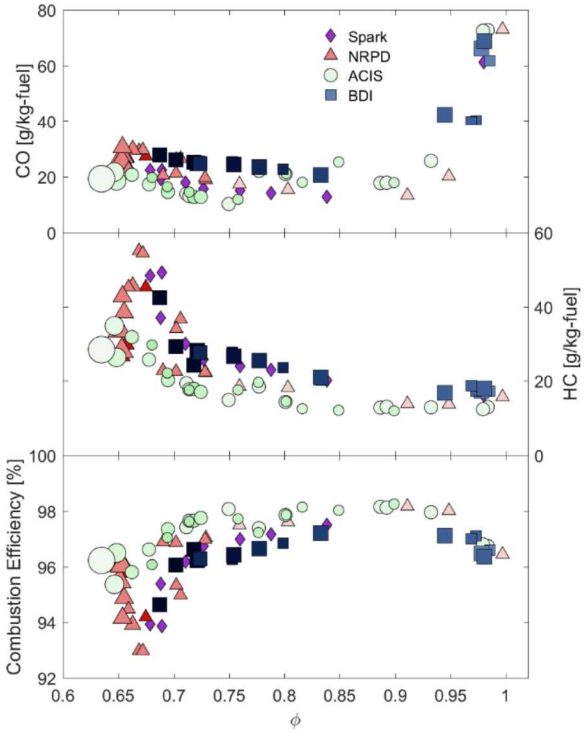

FIGURE 8: Carbon monoxide and unburned hydrocarbon emissions from different ignition systems, along with a comparison of combustion efficiency.

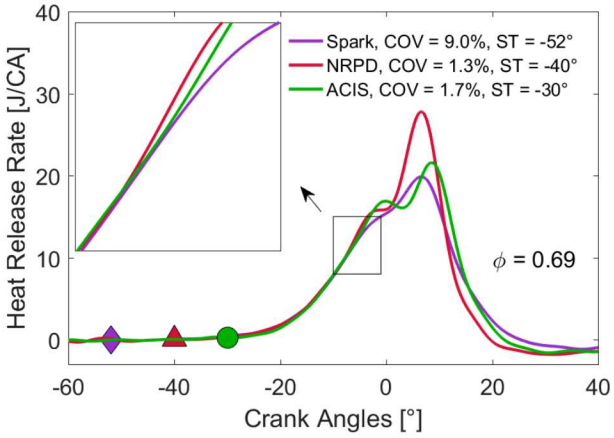

FIGURE 9. Close-up comparison of HRR profiles produces at a fixed lean equivalence ratio ($\phi = 0.69$) produced from spark, NRPD, and ACIS igniters.

4. CONCLUSIONS

The present study compares the performance and emissions characteristics of three different advanced ignition systems – ACIS, BDI, and NRPD; in a single-cylinder, optically accessible, research engine for a single operating condition, 1300 rpm, and 3.5 bar IMEP varying the equivalence ratio from stoichiometry to lean-limit. The ACIS and BDI used an RF pulse waveform for durations of between 300 to 2000 µs, while NRPD used DC nanosecond discharges at a fixed 100 kHz. Major findings are as follows:

- Lean stability limits of $\phi = 0.73$ for the inductive spark were extended for both the ACIS ($\phi = 0.68$) and NRPD ($\phi = 0.65$) igniters. The extended lean stability limit led to an associated increase in peak ITE from 32.5% for the spark igniter to 33.8% and 34.5% for ACIS and NRPD, respectively. Moreover, the lean stability limit was not reached during the limited test window for NRPD, which suggests further improvement is possible. The performance of BDI, however, was very close to the inductive spark.
- Increased pulse number for NRPD was highly effective for improving cyclic stability for the leanest mixtures (i.e., $\phi < 0.7$). Increased pulse duration was likewise effective for the ACIS system, but was limited by the lower in-cylinder densities for the leanest mixtures due to additional ST advance. The results suggest that ignition protrusion into the combustion chamber (and hence away from conductive metal surfaces) is an important parameter for combustion chamber optimization with ACIS.
- Large initial ignition kernels from the ACIS that resulted from corona streamer discharges into the bulk gas from the 4-prong electrode led to producing the fasted early burn rates of all ignition systems. As a result, ST could be retarded by 5 CA for stoichiometric mixtures and by as much as 20 CA for lean mixtures relative to the inductive spark ST, while still maintaining the same combustion phasing. Shorter combustion durations and an associated increase in combustion efficiency led to an additional 0.5 – 1.0 ITE points efficiency improvement.
- Ignition kernels for NRPD were augmented by successive pulses that added expansion energy to the kernel burned gas region, which was the critical parameter for expanded lean ignition limits.

Future studies will leverage available optical access into the engine and high-speed intensified cameras to visualize early flame kernel growth periods for LTP igniters. The use of BDI pre-strikes will also be investigated as a way to extend BDI dilution tolerance limits. Finally, the impact of dilution by exhaust gas recirculation with these igniters will be explored.

ACKNOWLEDGMENTS

The authors would like to thank Alberto Garcia, Gary Hubbard, and Keith Penney for their dedicated support of the Gasoline Combustion Fundamentals Laboratory. We would moreover like to thank Marco Mehl with his assistance in developing the 5-component gasoline surrogate. The work was performed at the Combustion Research Facility, Sandia National Laboratories, Livermore, CA. Financial support was provided by the U.S. Department of Energy, Vehicle Technologies Office. Sandia National Laboratories is a multi-mission laboratory managed and operated by National Technology and Engineering Solutions of Sandia, LLC., a wholly-owned subsidiary of Honeywell International, Inc., for the U.S. Department of Energy's National Nuclear Security Administration under contract DE-NA0003525.

REFERENCES

1. Rapp, V., N. Killingsworth, P. Therkelsen, and R. Evans, "*Lean-Burn Internal Combustion Engines,*" 2016: p. 111-146.
2. Gheorghiu, V., "*Ultra-Downsizing of Internal Combustion Engines*," in *Sustainable Automotive Technologies*, A. Subic, J. Wellnitz, M. Leary, and L. Koopmans, Editors. 2012, Springer, Berlin: Heidelberg.
3. Lecointe, B. and G. Monnier, "*Downsizing a Gasoline Engine Using Turbocharging with Direct Injection,*" SAE Technical Paper 2003-01-0542, 2003.
4. Golloch, R. and G.P. Merker, "*Internal combustion engine downsizing,*" MTZ Worldw, 2005. **66**: p. 20-22.
5. Dec, J.E., "*Advanced compression-ignition engines—understanding the in-cylinder processes,*" Proceedings of the Combustion Institute, 2009. **32**(2): p. 2727-2742.
6. Lawler, B.J. and Z.S. Filipi, "*Integration of a Dual-Mode SI-HCCI Engine Into Various Vehicle Architectures,*" Journal of Engineering for Gas Turbines and Power, 2013. **135**(5).
7. Weinrotter, M., E. Wintner, K. Iskra, T. Neger, J. Olofsson, H. Seyfried, M. Aldén, M. Lackner, F. Winter, A. Vressner, A. Hultqvist, and B. Johansson, "*Optical Diagnostics of Laser-Induced and Spark Plug Assisted HCCI Combustion,*" SAE Technical Paper 2005-01-0129, 2005.
8. Zhao, F., T.N. Asmus, D.N. Assanis, J.E. Dec, J.A. Eng, and P.M. Najt. "*Homogeneous Charge Compression Ignition (HCCI) Engines: Key Research and Development Issues*," in *Society of Automotive Engineers International*. 2003. Warrendale, PA.
9. Leonov, S.B. and D.A. Yarantsev, "*Plasma-induced ignition and plasma-assisted combustion in high-speed flow,*" Plasma Sources Science and Technology, 2007. **16**(1): p. 132-138.
10. Chintala, N., A.N. Bao, G.F. Lou, and I.V. Adamovich, "*Measurements of combustion efficiency in*

nonequilibrium RF plasma-ignited flows," Combustion and Flame, 2006. **144**(4): p. 744-756.
11. Sjöberg, M., W. Zeng, D. Singleton, J.M. Sanders, and M.A. Gundersen, "*Combined Effects of Multi-Pulse Transient Plasma Ignition and Intake Heating on Lean Limits of Well-Mixed E85 DISI Engine Operation,*" SAE International Journal of Engines, 2014. **7**(4): p. 1781-801.
12. Sun, W., M. Uddi, S.H. Won, T. Ombrello, C. Carter, and Y. Ju, "*Kinetic effects of non-equilibrium plasma-assisted methane oxidation on diffusion flame extinction limits,*" Combustion and Flame, 2012. **159**(1): p. 221-230.
13. Scarcelli, R., A. Zhang, and T. Wallner, "*Multi-dimensional modeling of non-equilibrium plasma for automotive applications,*" SAE Technical Paper 2018-01-0198, 2018.
14. Biswas, S., I. Ekoto, and R. Scarcelli, "*Transient Plasma Ignition (TPI) for Automotive Applications*," in *4th International Conference on Ignition Systems for Gasoline Engines*. 2018: Berlin.
15. Sevik, J., T. Wallner, M. Pamminger, R. Scarcelli, D. Singleton, and J. Sanders, "*Extending Lean and Exhaust Gas Recirculation-Dilute Operating Limits of a Modern Gasoline Direct-Injection Engine Using a Low-Energy Transient Plasma Ignition System,*" Journal of Engineering for Gas Turbines and Power, 2016. **138**(11): p. 1-9.
16. Cathey, C., J. Cain, H. Wang, and M.A. Gundersen, "*OH production by transient plasma and mechanism of flame ignition and propagation in quiescent methane-air mixtures,*" Combustion and Flame, 2008. **154**(4).
17. Starikovskiy, A. and N.L. Aleksandrov, "*Plasma-assisted ignition and combustion,*" Progress in Energy and Combustion Science, 2013. **39**(1): p. 61-110.
18. Gururajan, V., S. Scarcelli, A. Karpatne, D. Breden, L. Raja, S. Biswas, and I. Ekoto, "*A Computational Study of the Thermodynamic Conditions Leading to Autoignition in Nanosecond Pulsed Discharges,*" ICEF2019-7260, 2019.
19. Scarcelli, R., T. Wallner, S. Som, S. Biswas, I. Ekoto, D. Breden, A. Karpatne, and L. Raja, "*Modeling non-equilibrium discharge and validating transient plasma characteristics at above-atmospheric pressure,*" Plasma Sources Science and Technology, 2018. **27** (124006).
20. Singleton, D., S.J. Pendleton, and M.A. Gundersen, "*The role of non-thermal transient plasma for enhanced flame ignition in C2H4-air,*" Journal of Physics D: Applied Physics 2011. **44**(2): p. 022001-22002.
21. Nishiyama, A. and Y. Ikeda, "*Improvement of Lean Limit and Fuel Consumption Using Microwave Plasma Ignition Technology,*" SAE International Technical Paper, 2012. **2012-01-1139**.
22. Wolk, B., A. DeFilippo, J.Y. Chen, R. Dibble, A. Nishiyama, and Y. Ikeda, "*Enhancement of flame development by microwave-assisted spark ignition in constant volume combustion chamber,*" Combustion and Flame, 2013. **160**(7): p. 1225-1235.
23. Mintusov, E., A. Serdyuchenko, I. Choi, W.R. Lempert, and I.V. Adamovich, "*Mechanism of plasma assisted oxidation and ignition of ethylene–air flows by a repetitively pulsed nanosecond discharge,*" Proceedings of the Combustion Institute, 2009. **32**(2): p. 3181-3188.
24. Kosarev, I.N., N.L. Aleksandrov, S.V. Kindysheva, S.M. Starikovskaia, and A.Y. Starikovskii, "*Kinetics of ignition of saturated hydrocarbons by nonequilibrium plasma: CH□-containing mixtures,*" Combustion and Flame, 2008. **154**(3).
25. Biswas, S. and I. Ekoto, "*Detailed Investigation into the Effect of Ozone Addition on Spark Assisted Compression Ignition Engine Performance and Emissions Characteristics,*" SAE Technical Paper 2019-01-0966, 2019.
26. Biswas, S. and I. Ekoto, "*Spark Assisted Compression Ignition Engine with Stratified Charge Combustion and Ozone Addition,*" JSAE 20199089, 2019.
27. Chang, J., O. Güralp, Z. Filipi, D. Assanis, T.-W. Kuo, P. Najt, and R. Rask, "*New Heat Transfer Correlation for an HCCI Engine Derived from Measurements of Instantaneous Surface Heat Flux*." 2004, SAE Technical Paper 2004-01-2996.
28. Idicheria, C.A., H. Yun, and P.M. Najt, "*An Advanced Ignition System for High Efficiency Engines*," in *Ignition Systems for Gasoline Engines*. 2018: Berlin.
29. Cruccolini, V., G. Discepoli, F. Ricci, L. Petrucci, C. Grimaldi, S. Papi, and M. Dal Re, "*Comparative Analysis between a Barrier Discharge Igniter and a Streamer-Type Radio-Frequency Corona Igniter in an Optically Accessible Engine in Lean Operating Conditions,*" SAE Technical Paper 2020-01-0276, 2020.